

High-spin structures of $^{88}_{36}\text{Kr}_{52}$ and $^{89}_{37}\text{Rb}_{52}$: Evolution from collective to single-particle behaviors

A. Astier,¹ M.-G. Porquet,¹ Ts. Venkova,^{1,2} G. Duchêne,^{3,4} F. Azaiez,^{3,4,*} D. Curien,^{3,4}
I. Deloncle,¹ O. Dorvaux,^{3,4} B.J.P. Gall,^{3,4} N. Redon,⁵ M. Rousseau,^{3,4} and O. Stézowski⁵

¹*CSNSM, IN2P3-CNRS and Université Paris-Sud, Bât 104-108, F-91405 Orsay, France*

²*INRNE, BAS, 1784 Sofia, Bulgaria*

³*Université de Strasbourg, IPHC, 23 rue du Loess, F-67037 Strasbourg, France*

⁴*CNRS, UMR7178, F-67037 Strasbourg, France*

⁵*IPNL, IN2P3-CNRS and Université Claude Bernard, F-69622 Villeurbanne Cedex, France*

(Dated: October 12, 2018)

The high-spin states of the two neutron-rich nuclei, $^{88}\text{Kr}_{52}$ and $^{89}\text{Rb}_{52}$ have been studied from the $^{18}\text{O} + ^{208}\text{Pb}$ fusion-fission reaction. Their level schemes were built from triple γ -ray coincidence data and $\gamma - \gamma$ angular correlations were analyzed in order to assign spin and parity values to most of the observed states. The two levels schemes evolve from collective structures to single-particle excitations as a function of the excitation energy. Comparison with results of shell-model calculations gives the specific proton and neutron configurations which are involved to generate the angular momentum along the yrast lines.

PACS numbers: 23.20.Lv, 21.60.Cs, 27.50.+e, 25.85.Ge

I. INTRODUCTION

Many years ago, the systematics of nuclear ground state properties of long sequences of $_{38}\text{Sr}$, $_{37}\text{Rb}$ and $_{36}\text{Kr}$ isotopes were measured by laser spectroscopy [1–3]. They show that from $N = 50$, the magic gap, to $N = 58$, the mean square charge radii grow slowly, indicating small departures from spherical shape. This was confirmed by the behavior of the low-energy excitations of these nuclei. For instance the first two excited states of the even- Z $N = 52$ isotones with $Z = 32 - 38$ are those expected for a spherical harmonic vibrator: The 2_1^+ energies are less than 1 MeV and the $E(4_1^+)/E(2_1^+)$ ratios are close to 2. It is well known that along the yrast lines, the purely vibrational picture exhibited by nuclei near closed shells is perturbed by the admixture of other degrees of freedom, particularly the broken-pair states which provide large gain of angular momentum. That gives access to many proton and neutron configurations involving the high- j orbits close to the Fermi levels.

Nuclei with few protons above $Z = 28$ and few neutrons above $N = 50$ provide good testing grounds for the spherical shell model. Particularly, their high-spin states which are generated by aligning the angular momenta of broken nucleon pairs, can be clearly used to test some of the two-body matrix elements which are needed to predict the behavior of ^{78}Ni and its neighbors.

The present work reports on the study of the high-spin states of ^{88}Kr and ^{89}Rb using the $^{18}\text{O} + ^{208}\text{Pb}$ fusion-fission reaction. The level scheme of ^{88}Kr was extended up to 8-MeV excitation energy and several new transitions were added to the one of ^{89}Rb . Moreover $\gamma - \gamma$ an-

gular correlations were analyzed in order to assign spin and parity values to most of the high-spin states of these two $N = 52$ isotones. The comparison of the two level schemes with the predictions of shell-model calculations shows a good agreement. The analyses of the wave functions indicate that, except those of the first excited states which are very mixed, they are dominated by specific proton and neutron configurations, i.e., single-particle degrees of freedom of both protons and neutrons play a dominant role.

II. EXPERIMENTAL DETAILS

A. Reaction, γ -ray detection and analysis

We have used the $^{18}\text{O} + ^{208}\text{Pb}$ reaction at 85-MeV incident energy. The beam was provided by the Vivitron accelerator of IReS (Strasbourg). A 100 mg/cm² target of ^{208}Pb was used to stop the recoiling nuclei. The γ rays were detected with the Euroball array [4]. The spectrometer contained 15 Cluster germanium detectors placed in the backward hemisphere with respect to the beam, 26 Clover germanium detectors located around 90°, and 30 tapered single-crystal germanium detectors located at forward angles. Each Cluster detector consists of seven closely packed large volume Ge crystals [5] and each Clover detector consists of four smaller Ge crystals [6].

The data were recorded in an event-by-event mode with the requirement that a minimum of three unsuppressed Ge detectors fired in prompt coincidence. A set of 4×10^9 three- and higher-fold events was available for the subsequent analysis. The offline analysis consisted of both multi-gated spectra and three-dimensional 'cubes' built and analyzed with the Radware package [7].

* Present address: IPNO, IN2P3-CNRS and Université Paris-Sud, F-91406 Orsay, France.

More than one hundred nuclei are produced at high spin in such fusion-fission experiments, and this gives several thousands of γ transitions which have to be sorted out. Single-gated spectra are useless in most of the cases. The selection of one particular nucleus needs at least two energy conditions, implying that at least two transitions have to be known. This is the case of the yrast bands of the two nuclei of interest, ^{88}Kr and ^{89}Rb . We have nevertheless checked that their new transitions are detected in coincidence with those emitted by complementary fragments [8, 9]. For the reaction used in this work, we have studied many pairs of complementary fragments with known γ -ray cascades to establish the relationship between their number of protons and neutrons [10]. The sum of the proton numbers of complementary fragments has been found to be always the atomic number of the compound nucleus, $Z = 90$. The total number of emitted neutrons (sum of the pre- and post-fission neutrons) is mainly 4, 5, and 6.

B. γ - γ angular correlations

In order to determine the spin values of excited states, the coincidence rates of two successive γ transitions are analyzed as a function of θ , the average relative angle between the two fired detectors. The Euroball spectrometer had $C_{239}^2 = 28441$ combinations of 2 crystals, out of which ~ 2000 involved different values of relative angle within 2° . Therefore, in order to keep reasonable numbers of counts, all the angles have been gathered around three average relative angles : 22° , 46° , and 75° .

The coincidence rate is increasing between 0° and 90° for the dipole-quadrupole cascades, whereas it decreases for the quadrupole-quadrupole or dipole-dipole ones. More precisely, the angular correlation functions at the three angles of interest were calculated for several combinations of spin sequences, corresponding to typical multipole orders and their ratios are given in Table I. In order to check the method, angular correlations of transitions belonging to the yrast cascades of the fission fragments having well-known multipole orders were analyzed and the expected values were found in all cases.

III. EXPERIMENTAL RESULTS

A. Level scheme of $^{88}_{36}\text{Kr}$

The transitions deexciting the first two states of the yrast line of ^{88}Kr were identified many years ago from the β decay of ^{88}Br [11], establishing the 2_1^+ state at 775 keV and the 4_1^+ state at 1643 keV. More recently five new transitions deexciting medium-spin states were identified, following the spontaneous fission of ^{248}Cm [12].

The spectrum doubly-gated by the first two transitions of ^{88}Kr (at 775 and 868 keV) and built from our data

TABLE I. Values of the ratios of the angular correlation functions, $W(\theta)/W(75^\circ)$, computed for several combinations of spin sequences and multipole orders ($Q =$ quadrupole, $D =$ Dipole).

| Spin sequence $I_1 - I_2 - I_3$ | Multipole orders | $W(22^\circ)/W(75^\circ)$ | $W(46^\circ)/W(75^\circ)$ |
|------------------------------------|---------------------|---------------------------|---------------------------|
| 6-4-2 | $Q - Q$ | 1.13 | 1.06 |
| 6-5-4 | $D - D$ | 1.06 | 1.03 |
| 5-4-2 | $D - Q$ | 0.92 | 0.96 |
| 5-4-2 | $(D + Q)^a - Q$ | 0.73 | 0.88 |
| 5-4-2 | $(D + Q)^b - Q$ | 1.63 | 1.35 |
| 4-4-2 | $D - Q$ | 1.25 | 1.13 |

^a with a mixing ratio $\delta = -1$.

^b with a mixing ratio $\delta = +1$.

set, contains, in addition to these five transitions, a lot of other γ lines which are less intense. Therefore, we have analyzed all their coincidence relationships in order to build the level scheme which displays two independent parts lying above the 4_1^+ state at 1643 keV (see Fig. 1).

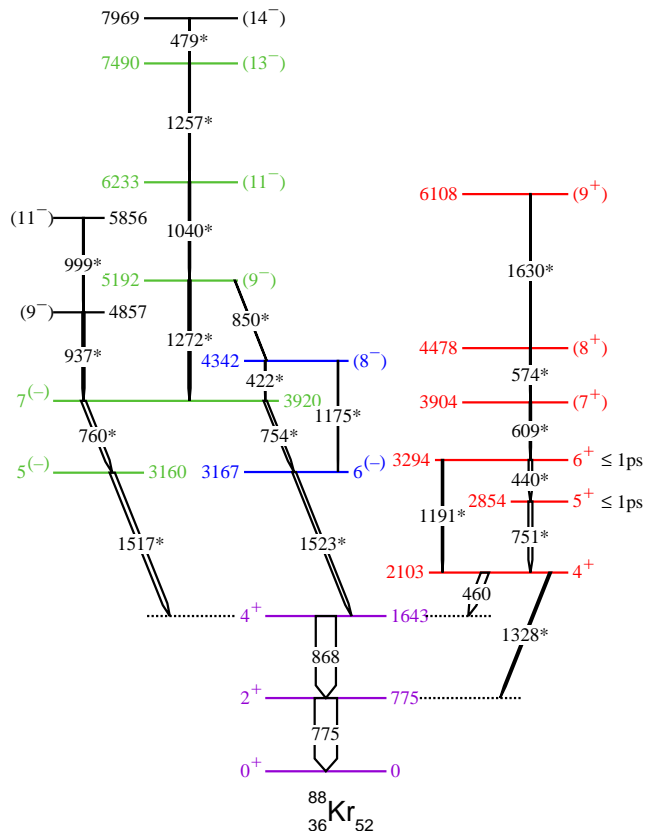


FIG. 1. (Color online) Level scheme of ^{88}Kr established in this work. Transitions, which are new or are placed differently as compared to Ref. [12], are marked with a star. The width of the arrows is proportional to the γ -ray intensity. The color code is the same as that of Fig. 7.

The 3920-keV level, belonging to the left part, is linked to the 4_1^+ state by means of two parallel cascades, 760-

1517 keV on the one hand and 754–1523 keV on the other hand. Because of their relative intensities, the order of the transitions of both cascades has to be inverted as compared to the previous work [12]. Moreover the fact that the 1175-keV transition is coincident with the 1523-keV transition and not with the 754-keV one confirms the order of the 754–1523 keV cascade. Two sets of coincident transitions are located above the 3920-keV level, (i) one set with two transitions of similar energies (937 and 999 keV) and (ii) one set with four transitions. An example of doubly-gated spectra showing the transitions belonging to this cascade is shown in Fig. 2.

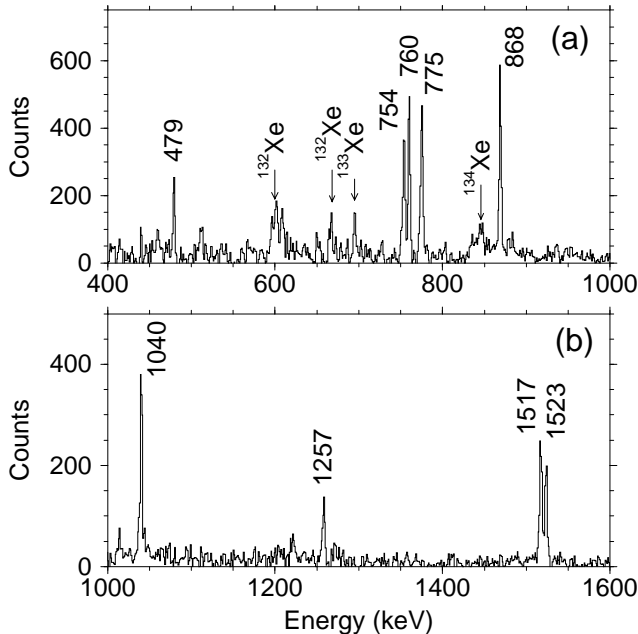


FIG. 2. Spectrum of γ rays in coincidence with two transitions of ^{88}Kr , the 1272- and the 868- or 775-keV transitions, (a) low energy part and (b) high energy part. Transitions emitted by $^{132-134}\text{Xe}$, the complementary fragments of ^{88}Kr , are labeled.

The right part of the level scheme is built on the 2103-keV level. It mainly decays to the 4_1^+ state by means of the 460-keV transition. Its link to the 2_1^+ state, newly observed in this work, is much weaker in intensity. The spectrum doubly-gated by the 1630-keV transition, located at the top of this new branch, and either the 868- or the 775-keV one is shown in Fig. 3.

Angular correlations of successive γ rays have been extracted for the most intense transitions of ^{88}Kr , provided that the $\gamma_i - \gamma_j$ coincidence of interest is not polluted. The experimental results are given in Table II.

Knowing that the 775- and 868-keV transitions have a stretched quadrupole character [12], these angular-correlation results show that both the 1523- and 760-keV transitions are quadrupole, while the 1517- and 754-keV ones are dipole. Thus the spin values of the 3160-, 3167- and 3920-keV states are 5, 6, and 7, respectively.

Regarding the right part of the level scheme, the 775–

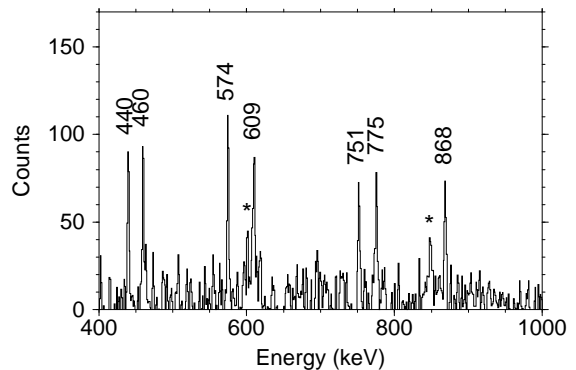


FIG. 3. Spectrum of γ rays in coincidence with two transitions of ^{88}Kr , the 1630- and the 868- or 775-keV transitions, showing the transitions belonging to the right part of the level scheme. The peaks marked with a star are contaminants.

TABLE II. Ratios of the coincidence rates between the low-lying γ rays of ^{88}Kr .

| γ - γ coincidence | $W(22^\circ)/W(75^\circ)^{(a)}$ | $W(46^\circ)/W(75^\circ)^{(a)}$ |
|---------------------------------|---------------------------------|---------------------------------|
| 775–1523 | 1.09(9) | 1.05(6) |
| 868–1523 | 1.2(1) | 1.1(1) |
| 775–760 | 1.17(9) | 1.03(6) |
| 775–1517 | 0.88(8) | 0.95(6) |
| 1523–754 | 0.89(8) | 0.95(6) |
| 775–460 | 1.23(8) | 1.15(6) |
| 868–460 | 1.18(8) | 1.06(6) |
| 775–440 | 0.82(7) | 0.92(5) |
| 460–440 | 0.92(7) | 0.94(5) |
| 751–440 | 1.09(7) | 1.05(6) |

^a The number in parentheses is the error in the last digit.

460 and 868–460 angular-correlation values would lead us to conclude that the 460-keV transition has a stretched quadrupole character, implying a $I^\pi = 6^+$ assignment for the 2103-keV level. Such a result is at variance with its decay to the 2_1^+ state (see Fig. 1). Thus the 460-keV transition is a $\Delta I = 0$ dipole transition, since such a transition gives comparable results as a $\Delta I = 2$ quadrupole one (see Table I). It is worth noting that the 2103-keV state has been populated with $L = 3$ or 4 in a transfer reaction [11], implying that it has either $I^\pi = 3^-$ or $I^\pi = 4^+$. The first value was already eliminated in Ref. [12] because it would imply a strong $E1$ decay to the 2_1^+ state, at variance with the experimental results. Thus, all these arguments result in $I^\pi = 4^+$ for the 2103-keV state. Finally, the last results of Table II indicate that the 440- and 751-keV transitions are dipole. Given that the 3294-keV state is directly linked to the 2103-keV state by means of the 1191-keV transition, this defines unambiguously the spin and parity values of the 2855- and 3295-keV states, $I^\pi = 5^+$ and 6^+ , respectively.

It is important to note that the 440- and 751-keV γ lines exhibit energy broadenings in spectra gated by tran-

sitions located below [see the red arrows in Figs. 4(a) and (b)]. Such shapes mean that the 440- and 751-keV transitions are partially emitted during the slowing-down of the ^{88}Kr fragments in the Pb target. Thus, the corresponding excited states do have half-lives ≤ 1 ps, i.e., $B(M1, 440 \text{ keV}) \geq 0.45 \mu_n^2$ and $B(M1, 751 \text{ keV}) \geq 0.09 \mu_n^2$.

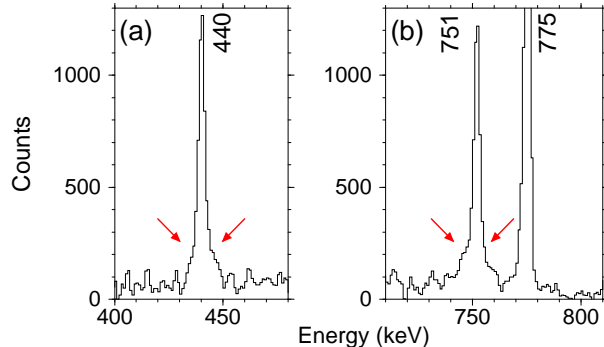


FIG. 4. (Color online) Spectrum of γ rays in coincidence with the 460- and 868-keV transitions. (a) the red arrows show the broadening of the 440-keV γ line. (b) the red arrows show the broadening of the 751-keV γ line.

Since the first states belonging to the right part of the level scheme have a positive parity, we have assumed that the states of the left part do have a negative parity (given in parentheses in Fig. 1). With such a choice, the 1523-keV transition would have a $M2$ character. Several $M2$ transitions are known in the $^{85,87,91}\text{Rb}$ isotopes [11], they deexcite isomeric states with various half-lives depending on the transition energies. Nevertheless all the $B(M2)$ values lie in a small range, $[4.4\text{--}10] 10^{-2}$ W.u.. Using these limits, the half-life of the 3167-keV level would be $T_{1/2} = 2\text{--}4$ ns, which is well below the time resolution of our apparatus [13].

Lastly, the spin assignments of the higher-lying states, given in parentheses, are based on the assumption that, in the yrast decays, spin values increase with excitation energy. We have gathered in Table III the properties of all the transitions assigned to ^{88}Kr from this work.

B. Level scheme of $^{89}_{37}\text{Rb}$

Our first results on high-spin states of ^{89}Rb were obtained when we were searching for the high-spin structure of the odd-odd ^{88}Rb nucleus [14] in the data set registered by the Eurogam array, following the $^{28}\text{Si} + ^{176}\text{Yb}$ reaction. The γ rays newly assigned to its neighbor, ^{89}Rb , were detected in coincidence with those of $^{109,110}\text{Ag}$ [15], their main complementary fragments in that fusion-fission reaction. The level scheme of ^{89}Rb built at that time extended up to 5326 keV and its main feature was the observation of the numerous transitions deexciting the 1195-keV level, already known from the β decay of ^{89}Kr [16]. Some years later, we quoted in a

TABLE III. Properties of the transitions assigned to ^{88}Kr observed in this work.

| E_γ^a (keV) | $I_\gamma^{a,b}$ | $I_i^\pi \rightarrow I_f^\pi$ | E_i | E_f |
|--------------------|------------------|-------------------------------|--------|--------|
| 421.6(4) | 3.0(15) | $(8^-) \rightarrow 7^{(-)}$ | 4342.2 | 3920.4 |
| 439.8(3) | 15(4) | $6^+ \rightarrow 5^+$ | 3294.2 | 2854.4 |
| 459.7(2) | 34(7) | $4^+ \rightarrow 4^+$ | 2103.2 | 1643.5 |
| 478.9(4) | 1.7(8) | $(14^-) \rightarrow (13^-)$ | 7969.0 | 7490.1 |
| 574.4(4) | 5(2) | $(8^+) \rightarrow (7^+)$ | 4478.1 | 3903.7 |
| 609.5(4) | 6(2) | $(7^+) \rightarrow 6^+$ | 3903.7 | 3294.2 |
| 751.2(3) | 17(4) | $5^+ \rightarrow 4^+$ | 2854.4 | 2103.2 |
| 753.7(3) | 13(3) | $7^{(-)} \rightarrow 6^{(-)}$ | 3920.4 | 3166.7 |
| 759.9(3) | 20(5) | $7^{(-)} \rightarrow 5^{(-)}$ | 3920.4 | 3160.5 |
| 775.1(2) | 100 | $2^+ \rightarrow 0^+$ | 775.1 | 0.0 |
| 850(1) | 1.5(7) | $(9^-) \rightarrow (8^-)$ | 5192.5 | 4342.2 |
| 868.4(2) | 90(13) | $4^+ \rightarrow 2^+$ | 1643.5 | 775.1 |
| 936.6(4) | 9.0(3) | $(9^-) \rightarrow 7^{(-)}$ | 4857.0 | 3920.4 |
| 999.2(4) | 4(2) | $(11^-) \rightarrow (9^-)$ | 5856.2 | 4857.0 |
| 1040.5(5) | 5(2) | $(11^-) \rightarrow (9^-)$ | 6233.0 | 5192.5 |
| 1175.5(7) | 2(1) | $(8^-) \rightarrow 6^{(-)}$ | 4342.2 | 3166.7 |
| 1191.2(5) | 6(2) | $6^+ \rightarrow 4^+$ | 3294.2 | 2103.2 |
| 1257.1(7) | 2.5(12) | $(13^-) \rightarrow (11^-)$ | 7490.1 | 6233.0 |
| 1272.1(5) | 10(3) | $(9^-) \rightarrow 7^{(-)}$ | 5192.5 | 3920.4 |
| 1328.1(5) | 7(2) | $4^+ \rightarrow 2^+$ | 2103.2 | 775.1 |
| 1517.0(4) | 21(4) | $5^{(-)} \rightarrow 4^+$ | 3160.5 | 1643.5 |
| 1523.2(4) | 17(4) | $6^{(-)} \rightarrow 4^+$ | 3166.7 | 1643.5 |
| 1630(1) | 1.5(7) | $(9^+) \rightarrow (8^+)$ | 6108 | 4478.1 |

^a The number in parentheses is the error in the last digit.

^b The relative intensities are normalized to $I_\gamma(775) = 100$.

publication related to the revised spin value of the ground state of its isotope, $^{87}\text{Br}_{52}$, that all the low-energy states of ^{89}Rb can be explained as collective states built on the deformed orbitals lying close to the $Z = 37$ Fermi level for a deformation $\epsilon \sim +0.15$ [17].

Later, the high-spin level scheme of ^{89}Rb was obtained by three groups, via various reactions induced by heavy ions [18–20]. The highest-energy state obtained in the first work is at 4033 keV [18], while the yrast line was extended up to 5605 keV in the second work [19] and 7391 keV in the third one [20]. It is worth mentioning that the two latter publications are conference proceedings, displaying only the obtained level scheme. Such a situation is summarized in a sentence of the abstract of the last compilation [21], “For ^{89}Rb , little information is available for high-spin structures”. The ^{89}Rb nucleus being well produced in the $^{18}\text{O} + ^{208}\text{Pb}$ reaction, we have resumed its study in order to get more precise information on its excited states.

An example of doubly-gated spectrum showing most of the transitions involved in the decay of the 1195-keV level is shown in Fig. 5. All the coincidence relationships have been carefully analyzed in order to produce the level scheme drawn in Fig. 6, which is in good agreement with the results of Ref. [20], except some points which are discussed now. We have inverted the order of the two highest-lying transitions, since the 686-keV transition has a higher intensity. A few other transitions have been

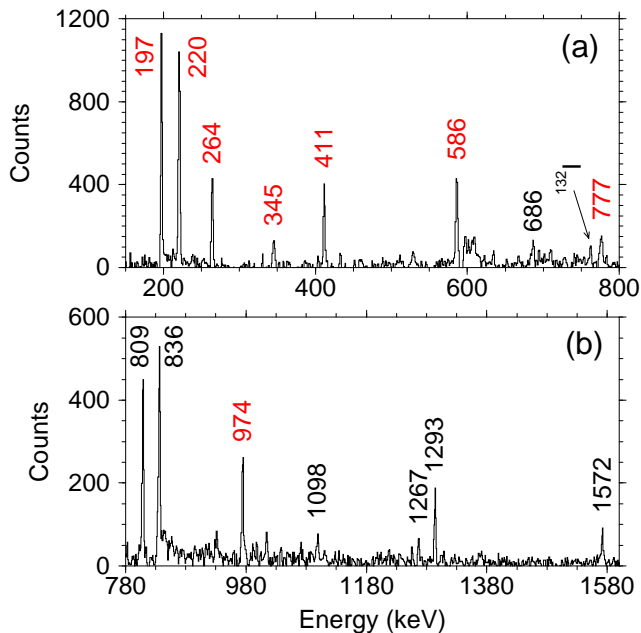


FIG. 5. (Color online) Spectrum of γ rays in coincidence with two transitions of ^{89}Rb , the 1193- and the 836- or 809-keV transitions. (a) low-energy part, (b) high-energy part. The γ -rays involved in the decay of the 1195-keV state are written in red. The transition emitted by ^{132}I , the main complementary fragment of ^{89}Rb in the $^{18}\text{O} + ^{208}\text{Pb}$ reaction, is labeled.

observed, such as the 1267- and 913-keV transitions in the high-spin part, and the 547- and 481-keV transitions in the low-spin part.

Angular correlations of successive γ rays have been extracted for the most intense transitions of ^{89}Rb . The experimental results are given in Table IV. They indicate that these transitions can be shared out between two groups with different multipole orders. The 197-, 220-, 411- and 586-keV γ rays belonging to the first one are dipole, while the 809-, 836-, 974-, and 1193-keV γ rays of the second one are quadrupole. Starting from the measured $3/2^-$ value of the ground state [11], this leads to the spin values of the 220-keV state ($5/2$), 586-keV state ($5/2$), 997-keV state ($7/2$), 1195-keV state ($9/2$), 2003-keV state ($13/2$), 2839-keV state ($17/2$), and 4032-keV state ($21/2$). Given that the 1195-keV state is isomeric, $T_{1/2} = 15.2(28)$ ns [19] or 8(2) ns [20], the quadrupole 974-keV transition has to be $M2$, implying that the 1195-keV state has a positive parity since the 220-keV state has a negative parity. In addition the spin-parity values of the 931-keV level, which is directly linked to the $9/2^+$ state and to the $3/2^-$ and $5/2_1^-$ states, is unambiguously $7/2^-$. All these spin and parity values are reported in Fig. 6 without parenthesis.

We have gathered in Table V the properties of all the transitions assigned to ^{89}Rb from this work. Before closing this section, it is important to note that the $B(M2; 9/2^+ \rightarrow 5/2^-)$ value of ^{89}Rb is $3.9(7) 10^{-2}$ W.u. or $7(2) 10^{-2}$ W.u. (depending on the half-life value [19,

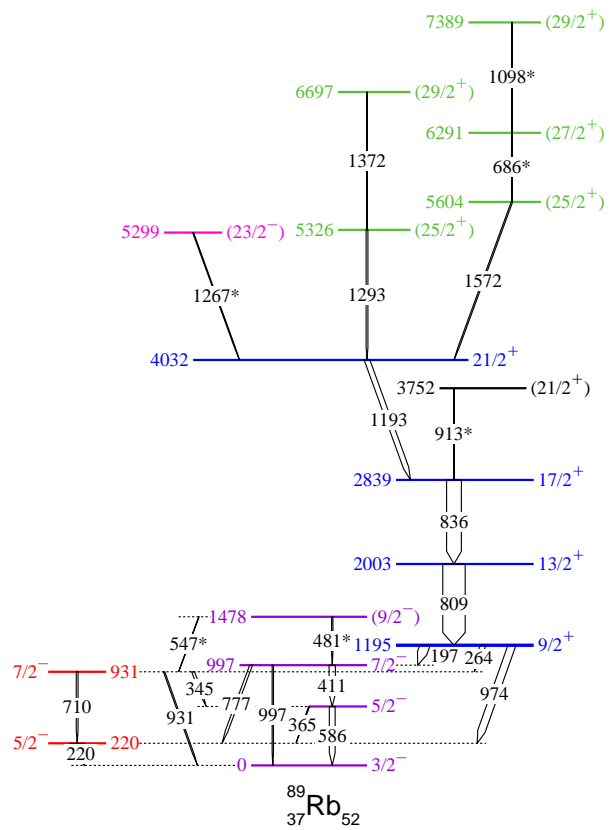


FIG. 6. (Color online) Level scheme of ^{89}Rb established in this work. The width of the arrows is proportional to the γ -ray intensity. Transitions, which are new or are placed differently as compared to Ref. [20], are marked with a star. The 1195-keV level is isomeric, $T_{1/2} = 15.2(28)$ ns [19] or 8(2) ns [20]. The color code is the same as that of Fig. 8.

TABLE IV. Ratios of the coincidence rates between the low-lying γ rays of ^{89}Rb .

| γ - γ coincidence | $W(22^\circ)/W(75^\circ)^{(a)}$ | $W(46^\circ)/W(75^\circ)^{(a)}$ |
|---------------------------------|---------------------------------|---------------------------------|
| 220-974 | 0.88(9) | 0.90(6) |
| 220-809 | 0.86(9) | 0.95(6) |
| 220-836 | 0.89(9) | 0.96(6) |
| 974-809 | 1.11(8) | 1.05(7) |
| 586-809 | 0.90(8) | 0.95(7) |
| 411-197 | 1.08(7) | 1.04(6) |
| 411-809 | 0.87(8) | 0.90(8) |
| 197-809 | 0.88(8) | 0.95(6) |
| 809-836 | 1.14(9) | 1.09(8) |
| 809-1193 | 1.11(9) | 1.08(8) |

^a The number in parentheses is the error in the last digit.

20]), i.e., in the same range than the ones of $^{85,87,91}\text{Rb}$ (see the values given at the end of Sect. III A).

TABLE V. Properties of the transitions assigned to ^{89}Rb observed in this work.

| E_γ^{a} (keV) | $I_\gamma^{\text{a,b}}$ | $I_i^\pi \rightarrow I_f^\pi$ | E_i | E_f |
|-----------------------------|-------------------------|---------------------------------|--------|--------|
| 197.4(2) | 43(9) | $9/2^+ \rightarrow 7/2^-$ | 1194.6 | 997.1 |
| 220.5(2) | 57(8) | $5/2^- \rightarrow 3/2^-$ | 220.5 | 0.0 |
| 263.8(2) | 23(5) | $9/2^+ \rightarrow 7/2^-$ | 1194.6 | 930.7 |
| 345.0(3) | 11(3) | $7/2^- \rightarrow 5/2^-$ | 930.7 | 585.7 |
| 365.4(4) | 3.0(15) | $5/2^- \rightarrow 5/2^-$ | 585.7 | 220.5 |
| 411.4(2) | 28(6) | $7/2^- \rightarrow 5/2^-$ | 997.1 | 585.7 |
| 481.4(4) | 3.0(15) | $(9/2^-) \rightarrow 7/2^-$ | 1478.5 | 997.1 |
| 547.5(8) | 2(1) | $(9/2^-) \rightarrow (7/2^-)$ | 1478.5 | 930.7 |
| 585.7(2) | 36(7) | $5/2^- \rightarrow 3/2^-$ | 585.7 | 0.0 |
| 686.5(5) | 3.8(16) | $(27/2^+) \rightarrow (25/2^+)$ | 6290.7 | 5604.2 |
| 710.2(4) | 8(2) | $7/2^- \rightarrow 5/2^-$ | 930.7 | 220.5 |
| 776.6(3) | 12(3) | $7/2^- \rightarrow 5/2^-$ | 997.1 | 220.5 |
| 808.8(2) | 100 | $13/2^+ \rightarrow 9/2^+$ | 2003.4 | 1194.6 |
| 836.1(2) | 65(10) | $17/2^+ \rightarrow 13/2^+$ | 2839.5 | 2003.4 |
| 912.8(4) | 6(2) | $(21/2^+) \rightarrow 17/2^+$ | 3752.3 | 2839.5 |
| 930.8(4) | 6(2) | $7/2^- \rightarrow 3/2^-$ | 930.7 | 0.0 |
| 974.3(3) | 34(7) | $9/2^+ \rightarrow 5/2^-$ | 1194.6 | 220.5 |
| 997.4(4) | 6(2) | $7/2^- \rightarrow 3/2^-$ | 997.1 | 0.0 |
| 1098.1(5) | 2(1) | $(29/2^+) \rightarrow (27/2^+)$ | 7388.8 | 6290.7 |
| 1192.6(3) | 25(5) | $21/2^+ \rightarrow 17/2^+$ | 4032.1 | 2839.5 |
| 1266.9(4) | 3.4(17) | $(23/2) \rightarrow 21/2^+$ | 5299.0 | 4032.1 |
| 1293.5(4) | 7.6(23) | $(23/2) \rightarrow 21/2^+$ | 5325.6 | 4032.1 |
| 1371.6(5) | 1.8(9) | $(27/2) \rightarrow (23/2)$ | 6697.2 | 5325.6 |
| 1572.1(4) | 4.7(19) | $(25/2^+) \rightarrow 21/2^+$ | 5604.2 | 4032.1 |

^a The number in parentheses is the error in the last digit.

^b The relative intensities are normalized to $I_\gamma(809) = 100$.

IV. DISCUSSION

A. Generalities

The characteristics of the first two excited states of many even- Z $N = 52$ isotones [11] are typical of a collective motion, namely that of a spherical harmonic vibrator. All the 2_1^+ excitation energies are less than 1 MeV, from 832 keV for $Z = 38$ to 624 keV for $Z = 32$, and all the $E(4_1^+)/E(2_1^+)$ ratios are close to 2. Nevertheless, such a behavior does not extend to higher angular momenta, where other sets of states appear.

The medium-spin states of the $N = 52$ isotones with $Z \sim 36$ then involve the breaking of nucleon pairs located in the various orbits located close to the Fermi levels. The two valence neutrons are likely in the $\nu d_{5/2}$ and/or $\nu g_{7/2}$ orbits just above the $N = 50$ shell gap. Regarding the protons, three orbits located between the $Z = 28$ and the $Z = 50$ shell gaps, $\pi f_{5/2}$, $\pi p_{3/2}$, and $\pi g_{9/2}$, are to be considered for the pair breakings in order to increase the value of angular momenta. Table VI gives various configurations of ^{88}Kr , with one and two broken pairs. Obviously some of the pure proton configurations have been already identified in $^{86}\text{Kr}_{50}$, such as the 4^+ state at 2250 keV, the 6^- state at 4430 keV, or the 7^- state at 4693 keV [23]. On the other hand, other ones, being not yrast, cannot be easily observed experimentally.

TABLE VI. Various configurations, expected in ^{88}Kr , with one or two broken pairs in the subshells close to the Fermi levels, sorted by order of I_{max}^π .

| Neutron pair | Proton pair | I_{max}^π | Seniority ($S_\nu + S_\pi$) |
|----------------------------------|---|---------------|----------------------------------|
| $(\nu d_{5/2})^2$ | — | 4^+ | 2 (2+0) |
| — | $(\pi f_{5/2})^1(\pi p_{3/2})^1$ | 4^+ | 2 (0+2) |
| — | $(\pi f_{5/2})^2$ | 4^+ | 2 (0+2) |
| $(\nu d_{5/2})^1(\nu g_{7/2})^1$ | — | 6^+ | 2 (2+0) |
| — | $(\pi g_{9/2})^2$ | 8^+ | 2 (0+2) |
| — | $(\pi f_{5/2})^2(\pi p_{3/2})^2$ | 6^+ | 4 (0+4) |
| $(\nu d_{5/2})^2$ | $(\pi f_{5/2})^1(\pi p_{3/2})^1$ | 8^+ | 4 (2+2) |
| $(\nu d_{5/2})^1(\nu g_{7/2})^1$ | $(\pi f_{5/2})^1(\pi p_{3/2})^1$ | 10^+ | 4 (2+2) |
| $(\nu d_{5/2})^2$ | $(\pi g_{9/2})^2$ | 12^+ | 4 (2+2) |
| — | $(\pi f_{5/2})^1(\pi p_{3/2})^1(\pi g_{9/2})^2$ | 12^+ | 4 (0+4) |
| $(\nu d_{5/2})^1(\nu g_{7/2})^1$ | $(\pi g_{9/2})^2$ | 14^+ | 4 (2+2) |
| — | $(\pi p_{3/2})^1(\pi g_{9/2})^1$ | 6^- | 2 (2+0) |
| — | $(\pi f_{5/2})^1(\pi g_{9/2})^1$ | 7^- | 2 (2+0) |
| $(\nu d_{5/2})^2$ | $(\pi p_{3/2})^1(\pi g_{9/2})^1$ | 10^- | 4 (2+2) |
| — | $(\pi f_{5/2})^2(\pi p_{3/2})^1(\pi g_{9/2})^1$ | 10^- | 4 (0+4) |
| $(\nu d_{5/2})^2$ | $(\pi f_{5/2})^1(\pi g_{9/2})^1$ | 11^- | 4 (2+2) |
| $(\nu d_{5/2})^1(\nu g_{7/2})^1$ | $(\pi p_{3/2})^1(\pi g_{9/2})^1$ | 12^- | 4 (2+2) |
| $(\nu d_{5/2})^1(\nu g_{7/2})^1$ | $(\pi f_{5/2})^1(\pi g_{9/2})^1$ | 13^- | 4 (2+2) |

It is likely the case of the 8^+ fully aligned state of the $(\pi g_{9/2})^2$ configuration, because of the high energy of the $\pi g_{9/2}$ orbit above the Fermi level (the excitation energy of the $9/2^+$ state of ^{85}Br is 1859 keV [13]). Similarly, the configuration involving the breaking of a $(\pi f_{5/2})^2$ pair is lying above the yrast line, since a proton pair has to be promoted from the fully occupied $\pi f_{5/2}$ orbit¹ into the $\pi p_{3/2}$ or $\pi p_{1/2}$ subshells. Nevertheless such proton-pair breakings must be involved in yrast states with higher seniority since this is the only way to gain extra values of angular momentum.

By using Table VI as a guide, the main configuration of some states of ^{88}Kr could be assigned. The 4^+ state lying at 2103 keV (see Fig. 1) likely comes from the breaking of a proton pair, $(\pi f_{5/2})^1(\pi p_{3/2})^1$, and the (8^+) state at 4478-keV excitation energy from the breaking of two pairs, $(\nu d_{5/2})^2(\pi f_{5/2})^1(\pi p_{3/2})^1$. The $6^{(-)}$ and $7^{(-)}$ states (lying at 3167 and 3920 keV, respectively) would involve a different proton pair, $(\pi p_{3/2})^1(\pi g_{9/2})^1$ and $(\pi f_{5/2})^1(\pi g_{9/2})^1$, respectively. Adding the breaking of the neutron pair, either $(\nu d_{5/2})^2$ or $(\nu d_{5/2})^1(\nu g_{7/2})^1$, we could explain the set of states lying above 3920 keV, up to $I^\pi = 13^-$.

¹ The proton configuration of the ^{88}Kr ground state is assumed to be $(\pi f_{5/2})^6(\pi p_{3/2})^2$.

A similar approach can be held for the high-spin states of ^{89}Rb , a proton being added in one of the orbits located between the $Z = 28$ and the $Z = 50$ shell gaps. The states, with a seniority of one, would be the $3/2^-$ ground state, the $5/2^-$ state at 220 keV and the $9/2^+$ state at 1195 keV, with the $(\pi p_{3/2})^1$, $(\pi f_{5/2})^1$, and $(\pi g_{9/2})^1$ configuration, respectively. The increase of angular momentum in each structure could be due to the breaking of one neutron pair or one proton pair. For instance, the $21/2^+$ state at 4032 keV (see Fig. 6) is likely the fully aligned state of the $(\nu d_{5/2})^1(\nu g_{7/2})^1(\pi g_{9/2})^1$ configuration. A proton pair has then to be broken in order to gain more angular momentum, implying that the states measured above 5 MeV excitation energy have likely a seniority of five.

Nevertheless, in order to have a better insight of the excitations involved in the high-spin states identified in ^{88}Kr and ^{89}Rb , particularly the respective roles of the neutrons and the protons, the shell-model approach has to be used because of the large number of possible configurations involved in the same range of excitation energy.

B. Results of shell-model calculations

We have performed shell-model (SM) calculations, using the interaction "glekpn" (described in Ref. [24]) and the NuShellX@MSU code [25]. The "glekpn" model space includes five proton orbits ($\pi f_{7/2}$, $\pi f_{5/2}$, $\pi p_{3/2}$, $\pi p_{1/2}$, $\pi g_{9/2}$) and five neutron orbits ($\nu g_{9/2}$, $\nu g_{7/2}$, $\nu d_{5/2}$, $\nu d_{3/2}$, $\nu s_{1/2}$), which is suitable for the description of nuclei with $20 < Z < 50$ and $40 < N < 70$. Due to the too large dimension of the valence space when $Z \sim 36$ and $N = 52$, the $\pi f_{7/2}$ and the $\nu g_{9/2}$ subshells were constrained to be fully occupied, meaning that excitations across the $Z = 28$ and the $N = 50$ gaps were forbidden for the calculations we have performed in the present work. The effects of such truncations will be appraised in the next sections, when discussing the main results of these SM calculations.

1. ^{88}Kr

The results of the SM calculations for ^{88}Kr are given in Fig. 7(a), showing only the states close to the yrast line. Above 2 MeV excitation energy, three sets of states are predicted. The first one starts at $I^\pi = 4^+$ and ends at $I^\pi = 10^+$ [see the red empty squares in Fig. 7(a)]. The two others have a negative parity, from $I^\pi = 5^-$ to $I^\pi = 13^-$ (see the green filled up-triangles) and from $I^\pi = 6^-$ to $I^\pi = 12^-$ (see the blue filled down-triangles).

The analysis of the wave functions allows us to identify which nucleon pairs are broken. For that purpose, we use (i) the values of the two components, I_p and I_n , which are coupled to give the total angular momentum of each state and (ii) for each I_p and I_n component, its decom-

position in terms of proton-neutron configurations, i.e., the occupation numbers of the eight valence orbits which are considered in the present calculations. Figs. 7(c-t) display the decomposition of the total angular momentum into the $I_p \otimes I_n$ components for each state of ^{88}Kr drawn in Fig. 7(a). Each percentage is written inside a square, drawn with an area proportional to it.

The major component of the 2_1^+ and 4_1^+ states comes from the breaking of the neutron pair, with $I_n = 2$ (57%) and 4 (68%), respectively (see Figs. 7(c-d), in violet). The breaking of a proton pair (with $I_p = 2$) is also involved in these two wave functions, the components being 28% and 20%.

The major part of the wave functions of the set of states from $I^\pi = 4_2^+$ to $I^\pi = 10^+$ (see Figs. 7(e-k) in red) has $I_p = 4$, coming from the first breaking of a proton pair, $(\pi f_{5/2})^1(\pi p_{3/2})^1$. In addition, the neutron component increases from $I_n = 0$ (for the 4_2^+ state) to $I_n = 6$ (for the 9^+ and 10^+ states). The 6^+ state of this set is the second one, the first one being predicted to lie at 3.316 MeV [see the black star in Fig. 7(a)]. The major component (89%) of this 6_1^+ state comes from two breakings, $I_n = 4 \otimes I_p = 2$.

The two sets of negative parity states have different proton configurations [see Figs. 7(l-t)]. The main components of the states with even- I (in blue) have an even value of I_p , while those of the odd- I states (in green) have an odd value of I_p . The increase of the total angular momentum of the states belonging to the two sets comes from the breaking of the neutron pair, from $I_n = 0$ to $I_n = 6$. Then the maximum values of the angular momentum for the two sets are $I^\pi = 12^-$ and $I^\pi = 13^-$, respectively.

The experimental energies (see Fig. 1), drawn in Fig. 7(b) using the same symbols as those of Fig. 7(a), show a good agreement with these predictions. Thus all the excited states lying above 2 MeV excitation energy mainly involve first the breaking of a proton pair ($I_p^\pi = 4^+$ for the positive-parity states and $I_p^\pi = 5^- - 7^-$ for the negative-parity ones), the increase of angular momentum inside each structure coming from the breaking of a neutron pair.

Nevertheless, it is important to note that the quasi-vibrational behavior of the first two excited states (drawn in violet) is not very well reproduced, since the energy of the 2_1^+ state is predicted too high (988 keV instead of 775 keV). This is likely due to the truncation of the model space which hinders many of the correlations needed to reproduce the low energy of this first excited state.

Noteworthy is the fact that the 9_2^- state, predicted by the calculations to lie at 5543 keV, has a very peculiar wave function. It shows many different components (25% of $2_n^+ \otimes 7_p^-$, 24% of $4_n^+ \otimes 6_p^-$, 20% of $4_n^+ \otimes 5_p^-$, 8% of $2_n^+ \otimes 8_p^-$, 7% of $0_n^+ \otimes 9_p^-$, ...), thus resembling a 'collective' state. It could be compared to the (9^-) experimental state at 4857 keV, i.e., 937 keV above the $7^{(-)}$ state (see Fig. 1), even though it is predicted too high in energy. One could similarly assume that it is due to the truncation of the

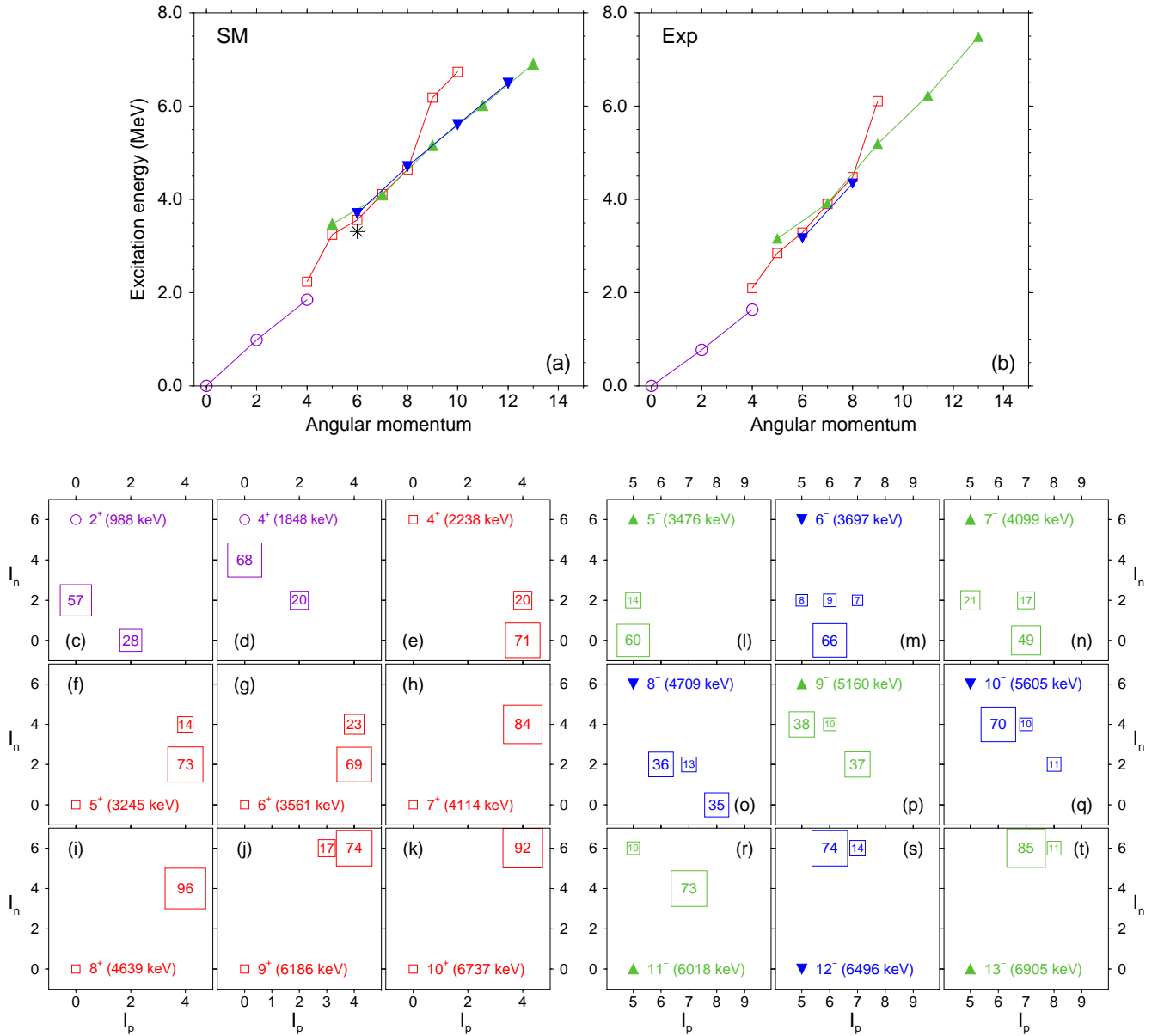


FIG. 7. (Color online) (a) Results of the shell-model calculations for ^{88}Kr (see text). The states having the same main configuration are linked by a solid line. (b) Experimental states of ^{88}Kr drawn with the same symbols as in (a). (c–t) For each state of ^{88}Kr drawn in (a), decomposition of its total angular momentum into the $I_p \otimes I_n$ components. Each percentage is written inside a square, drawn with an area proportional to it. Low percentages are not displayed. (c–k) positive-parity states, (l–t) negative-parity states.

model space.

Moreover, a 14^- state, with $I_p = 8 \otimes I_n = 6$ (87%) is predicted at 7963-keV excitation energy². The highest-spin state measured in this experiment has an excitation

energy very close to this prediction. Nevertheless its identification remains uncertain, as its distance in energy to the 13_1^- level is predicted too high (1058 keV as compared to 479 keV).

2. ^{89}Rb

The results of the SM calculations for ^{89}Rb are given in Fig. 8(a). As expected, the low-energy part of the level scheme displays three structures, built on the one-

² The $I_p = 8$ component comes from the breaking of two proton pairs, i.e., the partially aligned states of the two configurations, $(\pi f_{5/2})^2(\pi p_{3/2})^1(\pi g_{9/2})^1$ and $(\pi f_{5/2})^1(\pi p_{3/2})^2(\pi g_{9/2})^1$. The wave function of the 13^- state at 6905 keV contains also such a $I_p = 8$ component [see Fig. 7(t)].

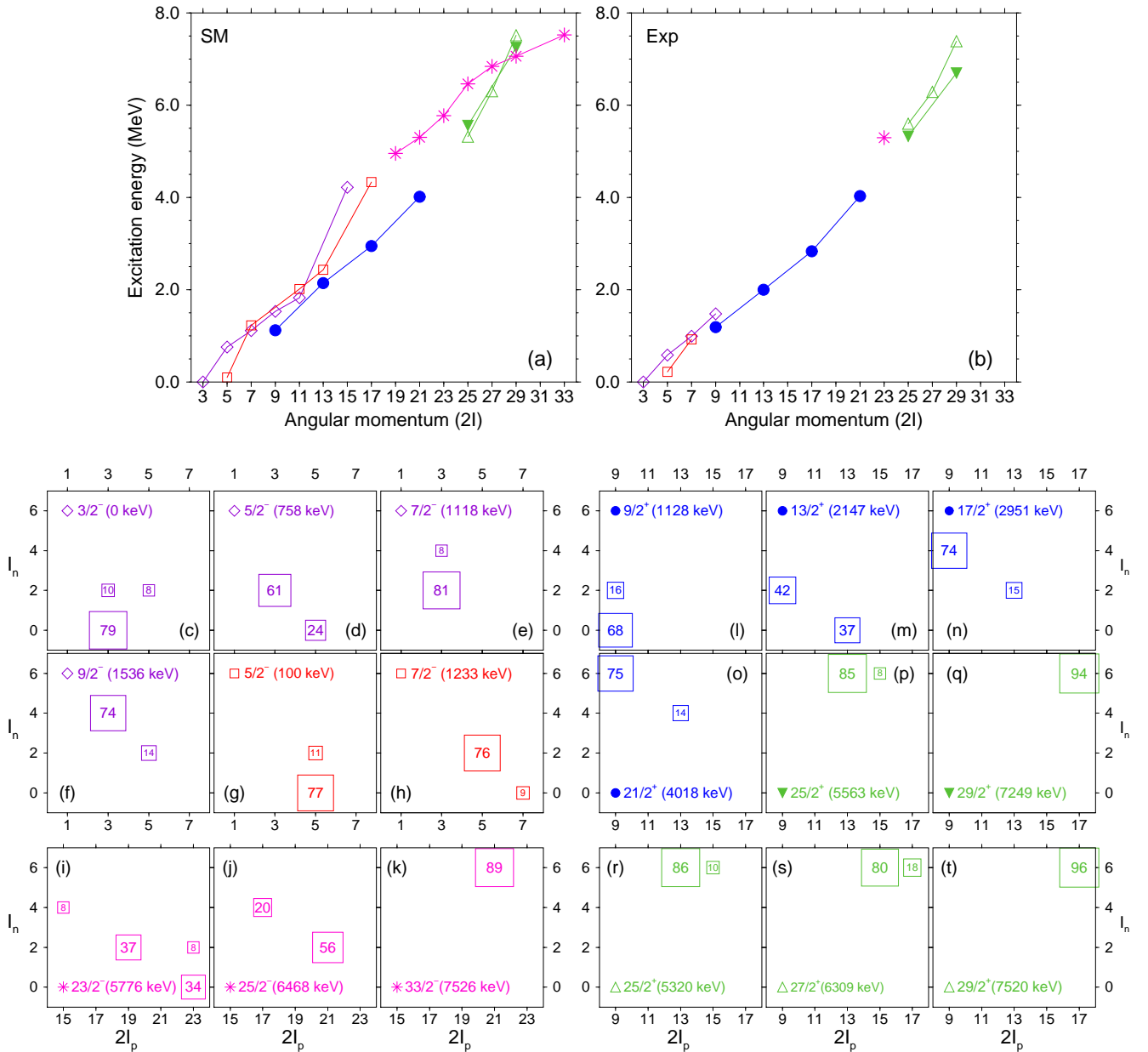


FIG. 8. (Color online) (a) Results of the shell-model calculations for ^{89}Rb (see text). The states having the same main configuration are linked by a solid line. (b) Experimental states of ^{89}Rb drawn with the same symbols as in (a). (c–t) For most of the states of ^{89}Rb drawn in (a), decomposition of their total angular momentum into the $I_p \otimes I_n$ components. Each percentage is written inside a square, drawn with an area proportional to it. Low percentages are not displayed. (c–k) negative-parity states, (l–t) positive-parity states.

proton configurations, $(\pi p_{3/2})^1$ (see the violet diamonds), $(\pi f_{5/2})^1$ (see the red squares), and $(\pi g_{9/2})^1$ (see the blue circles). The maximum values of the angular momentum, which are obtained when breaking the neutron pair ($I_n = 6$ from the $(\nu d_{5/2})^1(\nu g_{7/2})^1$ configuration), are $15/2^-$, $17/2^-$, and $21/2^+$, respectively.

In order to increase the angular momentum, another pair has to be broken. Three sets of states are then predicted at excitation energy higher than 5 MeV [see the magenta stars and the green triangles in Fig. 8(a)]. Since

their 29/2 states are close in energy, states from these three sets could be identified experimentally.

The coupling of the two components, I_p and I_n , to obtain the total angular momentum of the calculated states, are drawn in Figs. 8(c–t), which allows us to sort the states as a function of the I_p value of their main component. For instance, the band built on the $3/2^-$ ground state (79% with $I_p = 3/2$) comprises the $5/2_2^-$ (61%), $7/2_1^-$ (81%), and $9/2_1^-$ (74%) states (see Figs. 8(c–f), in violet). Similarly the main components of the $5/2_1^-$ and

$7/2^-$ state have $I_p = 5/2$ with 77% and 76%, respectively (see Figs. 8(g-h), in red). Regarding the positive-parity states above the $9/2^+$ state at 1128 keV, their main components have $I_p = 9/2$ (see Figs. 8(l-o), in blue).

The angular momentum couplings of the five positive-parity states lying above 5 MeV excitation energy are given in Figs. 8(p-t) (in green). The wave functions of the two $25/2^+$ states (predicted at 5563 and 5320 keV) have very similar components, the major one corresponding to $I_p = 13/2 \otimes I_n = 6$ (86% and 85%, respectively) and the minor one to $I_p = 15/2 \otimes I_n = 6$ (10% and 8%, respectively). This is the same for the two $29/2^+$ states (calculated at 7249 and 7520 keV), which exhibit a $I_p = 17/2 \otimes I_n = 6$ coupling (94% and 96%, respectively). Nevertheless these I_p values do not originate from the same proton configurations, as shown in Table VII, allowing us to associate the $25/2_1^+$, $27/2_1^+$, and $29/2_2^+$ states on the one hand [see the green empty up-triangles in Fig. 8(a)], and the $25/2_2^+$ and $29/2_1^+$ states on the other hand [see the green filled down-triangles in Fig. 8(a)]. It is worth noting that the $\pi f_{5/2}$ and $\pi p_{3/2}$ orbits contain an odd number of protons for the main proton configuration of the $25/2_1^+$, $27/2_1^+$, and $29/2_2^+$ states, while they contain an even number of protons for the other set of states.

Regarding the third set of states predicted above 5 MeV excitation energy [see the magenta stars in Fig. 8(a)], their wave functions are characterized by the occupation of the $\pi g_{9/2}$ orbit by two protons, the pair being broken so as to give their high values of I_p (see Figs. 8(h-k), in magenta). This set of states extends from $I^\pi = 33/2^-$ down to $I^\pi = 19/2^-$, the bottom of the structure being located well above the yrast line. Then, one can assume that only the high-energy part would be populated in experiments such as the present one. For instance, the $23/2^-$ state decays more likely to the $21/2_1^+$ state than to the $21/2^-$ state, because of the largest γ -ray energy.

The experimental energies (see Fig. 6) drawn in Fig. 8(b) using the same symbols as those of Fig. 8(a), show a good agreement with these predictions. In the bottom of the level scheme, the odd proton lies in one of the odd-parity orbit. For $I \geq 9/2$, the positive-parity states involving the occupation of the $\pi g_{9/2}$ orbit form the yrast line. This structure ends at $I^\pi = 21/2^+$ where the two neutrons bring the maximum angular momentum, $6\hbar$. The greater values of the angular momentum are then obtained by breaking a pair of proton. Three sets of states are predicted with different proton configurations, in agreement with the observation of three transitions populating the $21/2^+$ state at 4032 keV (see Fig. 6).

3. Conclusion

The set of the "glekpn" effective interactions describes well the high-spin states of the two $N = 52$ isotones

studied in the present work. The only weakness seems to be the energy of the first quadrupole excitation which is predicted slightly too high. The $E(2_1^+ \rightarrow 0_1^+)$ value is 988 keV instead of 775 keV in ^{88}Kr . A similar deviation is observed in ^{89}Rb when the odd proton lies in the $\pi g_{9/2}$ orbit, i.e., $^{89}\text{Rb} = ^{88}\text{Kr} \otimes (\pi g_{9/2})^1$: $E(13/2_1^+ \rightarrow 9/2_1^+) = 1019$ keV instead of 809 keV. A good description of such states would need the excitations of some nucleons across the $Z = 28$ and $N = 50$ shell gaps, which were not considered in the present work because of the too large dimensions of the valence space for $Z \sim 36$ and $N = 52$.

C. Collectivity of the $N = 52$ isotones

As said above, the appearance of several groups of coincident transitions having similar energies of 800–900 keV can be considered as a sign of the excitation of an harmonic vibrator. This means that many $N = 52$ isotones exhibit this collective behavior in the low-energy parts of their level schemes. It is the case of the even- Z isotones, as well as the $\pi g_{9/2}$ structure of ^{89}Rb discussed in the previous section. The latter can be considered as the weak coupling of a $g_{9/2}$ proton to the states of an harmonic vibrator, which is confirmed by the SM calculations which predict the other members of the expected multiplets at excitation energies close to the one-phonon and two-phonon energies [being not yrast, these states are not drawn in Fig. 8(a)]. For instance the $11/2_1^+$ state is predicted at 2129 keV, i.e., very close to the $13/2_1^+$ state, both from the weak coupling of the $\pi g_{9/2}$ to the one-phonon excitation. Similarly, the $15/2_1^+$ state is calculated at 3064 keV, that is only 113 keV above the $17/2_1^+$ state, both from the weak coupling of the $\pi g_{9/2}$ to the two-phonon excitation.

The low-lying negative-parity states of ^{89}Rb cannot be interpreted within the same approach, as they do not exhibit $\Delta I = 2$ sequences, but $\Delta I = 1$ ones (with $\Delta I = 2$ cross-over transitions). On the other hand, these states can be discussed in terms of a "rotor + quasiparticle" approach, forming two rotational structures, built on the $3/2^- [301]$ and $5/2^- [303]$ deformed states, respectively. For a deformation parameter, $\epsilon = 0.15$, the $Z = 37$ Fermi level is located on the $3/2^- [301]$ state, the $5/2^- [303]$ one lying just below it (see the Figure 5 of Ref. [22]).

It is interesting to discuss the case of the lighter $N = 52$ isotope, ^{87}Br . In order to explain the feeding of some medium-spin states of ^{87}Kr from the β -decay of the ^{87}Br ground state [17], its spin value has been recently reevaluated to be $5/2^-$ (instead of the previous value, $3/2^-$, chosen from systematics, particularly because of its neighboring semi-magic isotope, ^{85}Br). Following the simple rule for the filling of the deformed proton orbits, the $Z = 35$ Fermi level is then on the $5/2^- [303]$ state, which gives $I^\pi = 5/2^-$ for the ground state, in perfect agreement with the new value.

The results of the SM calculations of ^{87}Br corroborate

TABLE VII. Proton configurations of the positive-parity high-energy states of ^{89}Rb . Percentages greater than 5% are given and the greatest value of each state is underlined.

| Proton configuration | $25/2_1^+$ 5320 keV | $25/2_2^+$ 5563 keV | $27/2_1^+$ 6309 keV | $29/2_1^+$ 7249 keV | $29/2_2^+$ 7520 keV |
|--|------------------------|------------------------|------------------------|------------------------|------------------------|
| $(\pi f_{5/2})^5(\pi p_{3/2})^3(\pi p_{1/2})^0(\pi g_{9/2})^1$ | <u>32%</u> | 14% | <u>53%</u> | 11% | <u>41%</u> |
| $(\pi f_{5/2})^4(\pi p_{3/2})^4(\pi p_{1/2})^0(\pi g_{9/2})^1$ | 19% | <u>39%</u> | | <u>53%</u> | 13% |
| $(\pi f_{5/2})^5(\pi p_{3/2})^2(\pi p_{1/2})^1(\pi g_{9/2})^1$ | 8% | 9% | 20% | | 21% |
| $(\pi f_{5/2})^4(\pi p_{3/2})^3(\pi p_{1/2})^1(\pi g_{9/2})^1$ | 12% | 7% | 10% | 17% | 10% |
| $(\pi f_{5/2})^3(\pi p_{3/2})^4(\pi p_{1/2})^1(\pi g_{9/2})^1$ | | 10% | | | |

this spin value and predict two $\Delta I = 1$ structures built on the ground state and the $3/2^-$ first excited state (see the left part of Fig. 9).

V. SUMMARY

The two neutron-rich nuclei, ^{88}Kr and ^{89}Rb , have been produced as fission fragments in the fusion reaction $^{18}\text{O}+^{208}\text{Pb}$ at 85-MeV bombarding energy, their γ rays being detected using the Euroball array. Their high-spin level schemes were built up to ~ 8 MeV excitation energy by analyzing triple γ -ray coincidence data. Using γ - γ angular correlation results, spin and parity values were assigned to most of states observed in the two isotones below 4-MeV excitation energy. The behaviors of the yrast structures identified in this work have been discussed, first, in comparison with the general features known in the mass region. Then results of SM calculations using the "glekpn" effective interactions in the $\pi f_{5/2}p_{3/2}g_{9/2} \otimes \nu g_{7/2}d_{5/2}$ valence space have been successfully compared to the experimental results. They describe well the evolution from collective to single-particle behaviors of these two isotones. Thanks to the components of the wave functions, particularly the two values, I_p and I_n , coupled to give the total angular momentum of each state, the increase of the angular momentum along the yrast lines could be precisely analyzed by identifying what nucleon pairs are successively contributing. Lastly, the behavior of the yrast states of the lighter isotone, ^{87}Br , has been discussed using the SM calculations, which predict that its ground state has $I^\pi = 5/2^-$, in agreement with a recent experimental result.

SM calculations

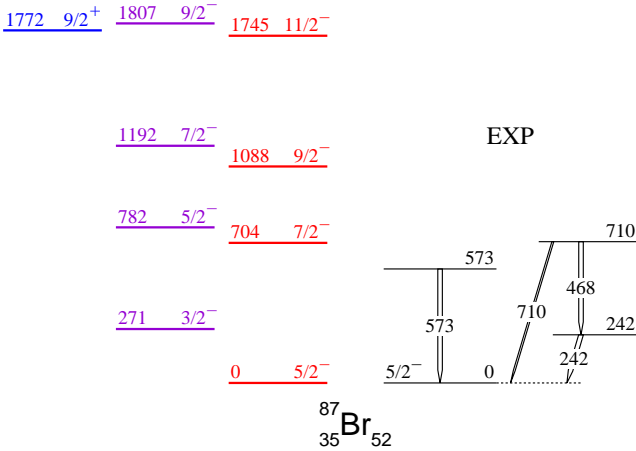


FIG. 9. (Color online) Levels of ^{87}Br predicted by the SM calculations, the color code is the same as the one of Fig. 8(a). The experimental states identified from the β -decay of ^{87}Se [26] are shown in the right part (the $5/2^-$ value of the ground-state spin is from Ref. [17]).

^{87}Br being in the heavy- A tail of the Br fragment distribution of the fusion-fission reaction used in the present work, its population is unfortunately too low to identify its yrast states using our data set. On the other hand, a few excited states were obtained from the β -decay of ^{87}Se studied many years ago [26]. The first three ones, drawn in the right part of Fig. 9, compare well with those predicted by the SM calculations. The 242-keV state is likely the $3/2^-$ band head, while the 573- and 710-keV levels would be the first members of the two collective structures.

ACKNOWLEDGMENTS

The Euroball project was a collaboration among France, the United Kingdom, Germany, Italy, Denmark and Sweden. The experiment was supported in part by the EU under contract HPRI-CT-1999-00078 (EURO-VIV). We thank many colleagues for their active participation in the experiments, Drs. A. Bogachev, A. Buta, F. Khalfalla, I. Piqueras, and R. Lucas. We thank the crews of the Vivitron. We are very indebted to M.-A. Saettle for preparing the Pb target, P. Bednarczyk, J. Devin, J.-M. Gallone, P. Médina, and D. Vintache for their help during the experiment.

-
- [1] F. Buchinger *et al.*, Phys. Rev. C **41**, 2883 (1990).
- [2] C. Thibault *et al.*, Phys. Rev. C **23**, 2720 (1981).
- [3] M. Keim *et al.*, Nucl. Phys. **A586**, 219 (1995).
- [4] J. Simpson, Z. Phys. A **358**, 139 (1997) and F. A. Beck Prog. Part. Nucl. Phys. A **28**, 443 (1992).
- [5] J. Eberth *et al.*, Nucl. Instrum. Methods **A 369**, 135 (1996).
- [6] G. Duchêne *et al.*, Nucl. Instrum. Methods **A 432**, 90 (1999).
- [7] D. Radford, Nucl. Instrum. Methods **A 361**, 297 and 306 (1995).
- [8] M.A.C. Hotchkis *et al.*, Nucl. Phys. **A530**, 111 (1991).
- [9] M.-G. Porquet *et al.*, Acta Phys. Polonica B **27**, 179 (1996).
- [10] M.-G. Porquet, Int. J. Mod. Phys. E **13**, 29 (2004).
- [11] ENSDF and XUNDL databases, <http://www.nndc.bnl.gov/ensdf/>.
- [12] T. Rząca-Urban *et al.*, Eur. Phys. J. A. **9**, 165 (2000).
- [13] A. Astier *et al.*, Eur. Phys. J. A. **30**, 541 (2006).
- [14] M.-G. Porquet, *Proceedings of the second International Conference on Fission and Properties of Neutron-Rich Nuclei, St Andrews, Scotland (1999)*, World Scientific (2000) p. 116.
- [15] M.-G. Porquet *et al.*, Eur. Phys. J. A. **15**, 463 (2002).
- [16] E.A. Henry, W.L. Talbert, and J.R. McConnell, Phys. Rev. C **7**, 222 (2073).
- [17] M.-G. Porquet *et al.*, Eur. Phys. J. A. **28**, 153 (2006).
- [18] D. Bucurescu *et al.*, Phys. Rev. C **76**, 064301 (2007).
- [19] D.A. Torres *et al.*, *Proceedings of the fourth International Workshop on nuclear fission and fission-product spectroscopy (2009)*, AIP Conference Proceedings 1175 (2009) p. 162.
- [20] T. Pawlat *et al.*, Acta Phys. Polonica B **40**, 629 (2009).
- [21] B. Singh, Nucl. Data Sheets **114**, 1 (2013).
- [22] M.-G. Porquet *et al.*, Phys. Rev. C **84**, 054305 (2011).
- [23] A. Prévost *et al.*, Eur. Phys. J. A. **22**, 391 (2004).
- [24] H. Mach *et al.*, Phys. Rev. C **41**, 226 (1990).
- [25] B.A. Brown, W.D.M. Rae, E. McDonald and M. Horoi, NuShellX@MSU, <http://www.nscl.msu.edu/~brown/resources/resources.html>.
- [26] M. Zendel, N. Trautmann, G. Hermann, J. Inorg. Chem. **42**, 1387 (1980).